ACS APPLIED POLYMER MATERIALS

pubs.acs.org/acsapm Article

Electrochemical Detection of Glutamate and Histamine Using Redox-Labeled Stimuli-Responsive Polymer as a Synthetic Target Receptor

Leila Ahmadian-Alam, Arturo Andrade, and Edward Song*

Cite This: ACS Appl. Polym. Mater. 2024, 6, 5630−5641 Read Online

ACCESS | Metrics & More | Article Recommendations | Supporting Information

ABSTRACT: Glutamate (Glu) and histamine (His) are two major neurotransmitters that play many critical roles in brain physiological functions and neurological disorders. Therefore, specific and sensitive monitoring of Glu and His is essential in the diagnosis and treatment of various mental health and neurodegenerative disorders. Both being nonelectroactive species, direct electrochemical detection of Glu and His has been challenging. Herein, we report a stimuli-responsive polymer-based biosensor for the electrochemical detection of Glu and His. The polymer-based target receptors consist of a linear chain stimuli-responsive templated polymer hybrid that is labeled with an osmium-based redox-active reporter molecule to elicit conformation-dependent electrochemical responses. The polymers are then attached to a gold electrode to implement an electrochemical sensor. The cyclic voltammetry (CV) and square-wave voltammetry (SWV) results confirmed the polymers' conformational changes due to the specific target (i.e., Glu and His) recognition and the corresponding electrochemical detection capabilities. The voltammetry results indicate that this biosensor can be used as a "signal-on" and "signal-off" sensors for the detection of Glu and His concentrations, respectively. The developed biosensor also showed excellent regeneration capability by fully recovering the initial current signal after being rinsed with deionized water. To further validate the polymer's utility as a target bioreceptor, the surface plasmon resonance (SPR) technique was used to characterize the binding affinity between the designed polymers and the target chemical. The SPR results exhibited the equilibrium dissociation constants (K_D) of 2.40 μM and 1.54 μM for the polymer−Glu and polymer−His interactions, respectively. The results obtained in this work strongly suggest that the proposed sensing technology could potentially be used as a platform for monitoring nonelectroactive neurochemicals from animal models.

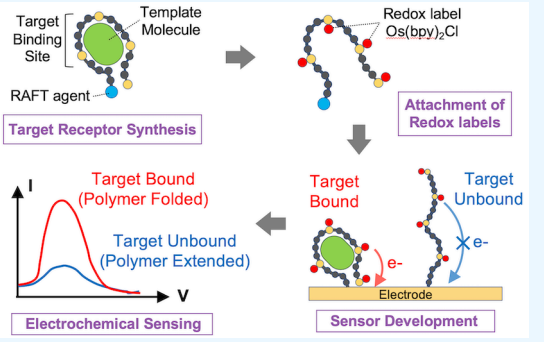

KEYWORDS: *Neurotransmitters, Templated polymers, Glutamate, Histamine, Electrochemical biosensor, SPR*

1. INTRODUCTION

Stimuli-responsive polymers are a unique class of polymer materials that have recently gained much attention in the chemical and biological sensing applications because they can undergo a binding-induced conformational change, which is reminiscent of the folding of functional nucleic acids such as aptamers due to specific binding to the target molecules.[1−3] Linear chain biomolecules such as aptamers have been widely used as key recognition element in many biomedical applications, especially in biosensing, due to their high sensitivity, rapid response, real-time detection capability, and easy operation.[4−7] However, the screening of highly specific and selective aptamers in an acceptable period of time and the difficulty in recognizing small molecules remain as main challenges of aptamer-based biosensors.[8] Hence, many efforts have been focused on finding alternative approaches to creating specific target receptors. Among the potential candidates introduced so far, the synthetic stimuli-responsive polymers,[1−3] elastin-like polypeptide (ELP),[9,10] and metal−organic framework (MOF)-based nanoparticles[11,12] are showing promising results for being used as alternative bioreceptors. Among these, the stimuli-responsive polymer's ability to change conformation upon target binding has made this class of polymers a rational alternative to DNA- or RNA-based aptamers.

Poly(*N*-isopropylacrylamide) (PNIPAM), as a merit example of stimuli-responsive polymers, has gained popularity because it provides a clear phase transition in the water around the human body temperature.[13] The lower critical solution temperature (LCST) phase behavior of PNIPAM gives rise to

Received: January 13, 2024
Revised: April 30, 2024
Accepted: May 2, 2024
Published: May 10, 2024

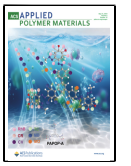

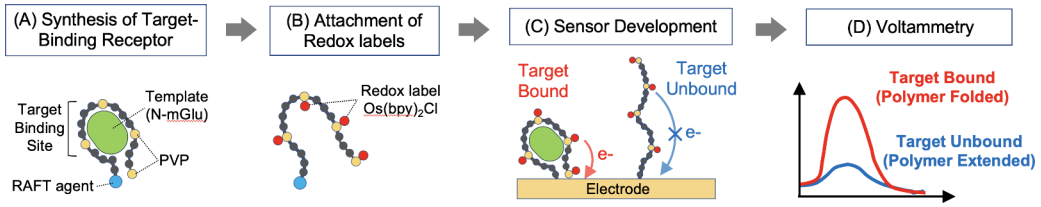

Figure 1. Schematic illustration of the proposed target-selective biosensing platform. (A) A linear-chain stimuli-responsive polymer is templated with a target molecule during RAFT polymerization to create target-specific affinity. (B) After polymer synthesis and template removal, the redox-active molecules (osmium complex, $Os(bpy)_2Cl$) are attached to the vinylpyridine (VP) in the polymer backbone. (C) When the redox-labeled polymers are grafted to the electrode, the target binding event induces a conformational change of the polymer from an extended to a folded state resulting in a higher electron transfer rate compared to an unbound polymer chian due to the relative position of the redox labels with respect to the electrode. (D) Applying voltammetry allows for target concentration-dependent sensor response due to the shape-changing behavior of the polymer-based target receptors.

a conformational switch from a shrunken and coiled conformation to a swollen and stretched chain conformation, thereby leading to different behaviors, properties, and responses for this polymer.[14] Various readout methods, such as electrochemistry,[15] colorimetry,[16] chemiluminescence,[17] fluorescence,[18] and surface plasmon resonance (SPR),[19] have been considered to convert a conformational switch-induced recognition response into a measurable signal in the literature relating to the aptamer-based biosensor design. However, the electrochemistry approach has gained particular attention compared to other successful methods due to its high sensitivity and rapid response. For this purpose, different strategies have been developed and used to incorporate signal-producing tags in the polymer backbone using polymerization of the polymerizable redox tag[20] and postfunctionalization.[21] The use of the polymerizable monomers already connected to the redox species, such as ferrocene and methylene blue, during polymerization is known as a straightforward approach to achieving a polymer with pendant redox labels.[20,21] In another approach, metal complex-based redox species such as ruthenium[22] and osmium[23] have been grafted to the polymer backbone through physical or chemical attachment.

In electrochemical biosensor design, the conformational changes of the redox-tagged polymer chains caused by the specific binding of the target molecules lead to a distance variation between the redox species and the electrode surfaces, thereby amplifying (signal-on) or quenching (signal-off) the output signal produced by the redox probe.[24−26] However, selective detection remains a challenge in the development of this type of biosensor platform. The highly selective polymeric receptor can be created by the conventional molecular imprinting approach.[27,28] However, the permanent cross-linking bonds between polymer chains produced by this method result in a rigid polymer structure and therefore restrict target recognition as well as the conformation switching capability of the polymers.[27,28] To address this issue, our strategy is to remove or minimize interchain polymer cross-linking to create a flexible and conformation changing linear polymer chain templated with target molecules to create a synthetic target receptor.[1,2] In this regard, we synthesized a single-chain stimuli-responsive templated PNIPAM-based receptor in our previous work and investigated its capability in the selective detection of nitrophenol derivatives.[1] Our findings supported the selective detection behavior of the templated PNIPAM-based receptor in detecting the template analyte used to synthesize the polymer and the polymer conformation change capability of the synthesized polymer-based receptor.[1]

Neurotransmitters, as messenger chemicals in our body, play many key roles in the functionalities of human physiology, most notably in the central and peripheral nervous system, brain activities, and mental health to name a few.[29,30] Thus, the development of a technique that can quantify and monitor the dynamics of neurotransmitters with high spatiotemporal resolution has recently become one of the most interesting and urgent areas of research. Literature review reveals that many efforts had been directed toward measuring redox-active neurotransmitters such as dopamine, serotonin, and adrenaline by electrochemical analysis, which rely on their nature of redox activity.[31] In contrast, electrochemical detection of non-electroactive neurochemicals such as glutamate (Glu)[32−34] and histamine (His),[35,36] have been challenging and often relies on an enzymatic approach which has some limitations such as lack of stability, susceptibility to environmental changes, and high cost.

These findings motivated us to design a redox-labeled templated poly(NIPAM)-based biosensor to monitor neurotransmitters Glu and His (Figure 1). In this work, the osmium-based redox label was chosen because of its oxidation at a safe potential window of 0−0.6 V vs Ag/AgCl, which is highly compatible with gold electrodes. Furthermore, another key benefit of using osmium complex as a redox label is that it can be grafted to the polymer after the templating step is complete, thereby eliminating the risk of the redox labels interfering with the target templating procedure. This ensures that target binding sites are formed with high fidelity with minimum contamination or corruption. We have synthesized a target-templated and redox-tagged poly[NIPAM-VP-MAA]-*g*-$Os(bpy)_2Cl$ hybrid that consists of NIPAM, vinylpyrridine (VP), and methacrylic acid (MAA) that form the molecular binding site and have the capability to undergo conformational changes upon target recognition. In addition, the osmium complex $Os(bpy)_2Cl$ attached to the polymer generates a label-free electrochemical response when the polymer conformation changes (Figure 1). After the polymer synthesis, we have confirmed and characterized the effective binding affinity between the polymer-based receptor and the target analyte using electrochemical analysis and the surface plasmon resonance (SPR) techniques.

2. EXPERIMENTAL SECTION

2.1. Materials. Methacrylic acid (MAA, 99%, Sigma-Aldrich), 2,2-azobis(isobutyronitrile) (AIBN, 98%, Sigma-Aldrich), 4-vinylpyridine (VP, ≥95%, Sigma-Aldrich), *N*-isopropylacrylamide (NIPAM, 97%, Sigma-Aldrich), 2-(dodecylthiocarbonothioylthio)-2-methylpropanoic acid (DDMAT, 98%, Sigma-Aldrich), *N*-methyl-L-glutamic acid (*N*-

https://doi.org/10.1021/acsapm.4c00121
ACS Appl. Polym. Mater. 2024, 6, 5630−5641

mGlu), L-glutamic acid (Glu, 99%, Sigma-Aldrich), histamine (≥97%, Sigma-Aldrich), serotonin hydrochloride (5-HT, Sigma-Aldrich), dopamine hydrochloride (DA, Sigma-Aldrich), 1,4-dioxane (anhydrous, 98%, Sigma-Aldrich), sodium sulfate (≥99%, Sigma-Aldrich), γ-aminobutyric acid (GABA, ≥99%, Sigma-Aldrich), tris(2-carboxyethyl)phosphine hydrochloride (TCEP, Sigma-Aldrich), 5,5′-dithio-bis(2-nitrobenzoic acid) (DTNB, 99%, Sigma-Aldrich), sodium perchlorate ($NaClO_4$, Fisher Scientific), phosphate buffered saline (PBS, Fisher Scientific), bovine serum albumin (BSA, Sigma-Aldrich), dimethyl sulfoxide (DMSO, ≥99.9%, ethanol (Fisher Scientific), sodium hydroxide (NaOH, ≥98%, Sigma-Aldrich), K_2OsCl_6 (99%, Alfa Aesar), 2,2′-bipyridine (bpy, 98%, Aldrich), ethyl ether (≥99%, Sigma-Aldrich), ethylene glycol (anhydrous, 99.8%, Sigma-Aldrich), and *N*,*N*-dimethylformamide (DMF, 99.8%, Sigma-Aldrich) were used without further purification.

2.2. Electrochemical Instrumentation. A three-electrode electrochemical cell consists of a gold electrode with diameter of 3 mm (BASi) as a working electrode, a platinum wire (BASi) as a counter electrode, and Ag/AgCl as a reference electrode (BioLogic: RE-1B) was set up within a Faraday cage (Gamry) to perform electrochemical analyses. A BioLogic VSP potentiostat was used to study the CV and SWV analyses.

2.3. Synthesis of $Os(bpy)_2Cl_2$ Complex. The $Os(bpy)_2Cl_2$ complex was synthesized based on previously reported procedure.[23] 2,2′-Bipyridine (0.62 mmol, 97 mg) and K_2OsCl_6 (0.31 mmol, 150 mg) were dissolved in 10 mL of DMF and stirred at 140 °C for 3 h. The KCl crystals that appeared upon cooling to room temperature were removed by paper filtration. Afterward, ethanol (5 mL) and ethyl ether (40 mL) were added to the remaining solution to precipitate the $Os(bpy)Cl_3.H_2O$ complex powder. Then, the $Os(bpy)Cl_3.H_2O$ powder was collected by centrifugation and dried in the air overnight. This powder was again dissolved in a mixture of H_2O/DMF/methanol (20 mL:2 mL:1 mL). Next, a saturated $Na_2S_2O_4$ solution was added to this solution to precipitate and obtain the $Os(bpy)_2Cl_2$ complex powder. Finally, the $Os(bpy)_2Cl_2$ powder was dried in a vacuum oven at 50 °C for 48 h.

2.4. Synthesis of Poly(NIPAM-VP-MAA) Copolymers. A PNIPAM-based random copolymer was synthesized based on the previously described protocol.[1,2] NIPAM (3.2 g, 28.5 mmol), MAA (0.32 mL, 3.75 mmol), VP (0.56 mL, 5.25 mmol), *N*-mGlu (64 mg, 0.39 mmol), and DDMAT (0.136 g, 0.37 mmol) were added to 25 mL of dioxane. This mixture was degassed and backfilled with N_2 gas for 5 min. Afterward, the AIBN initiator (30 mg, 0.18 mmol) was added to the mixture followed by placing this solution into an oil bath at 80 °C to start copolymerization and stirring at this temperature for 24 h. The poly(NIPAM-VP-MAA) copolymer powder was then precipitated into cold ethyl ether and collected by centrifuging. The copolymer powder was washed with cold ethyl ether several times until the ethyl ether solvent was colorless. The copolymer powder was dried under reduced pressure at 40 °C. For further purification, the copolymer powder was dissolved in deionized (DI) water and poured into the dialysis tubing with a molecular weight cutoff (MWCO) of 1 kDa. Then, the dialysis tubing was immersed in DI water for 3 days, and the water bath was changed every 4 h. After this step, the polymer solution was stirred at 50 °C to remove water and placed in a vacuum oven at 40 °C for 24 h.

2.5. Synthesis of Osmium-Grafted Copolymer Poly(NIPAM-VP-MAA)-*g*-$Os(bpy)_2Cl$. The synthesized poly(NIPAM-VP-MAA) copolymer (300 mg) and the $Os(bpy)_2Cl_2$ complex (180 mg) were dissolved in 5 mL of ethylene glycol and stirred at 140 °C for 24 h under a blanket of N_2 gas. This resulted in the attachment of the osmium complex on the copolymer backbone due to PVP-osmium chelation. After completing the reaction, the solution was poured into the dialysis tubing with a 1 kDa molecular weight cutoff (MWCO) to remove the unreacted $Os(bpy)_2Cl_2$. Then, the dialysis tubing was inserted into DI water for 3 days. The water bath was changed every 4 h. The polymer solution was stirred at 40 °C to remove water, and then, osmium-grafted polymer powder was placed into a vacuum oven at 40 °C for 24 h.

2.6. Ellman's Assay. The free thiol content of the synthesized poly(NIPAM-VP-MAA) was estimated by Ellman's assay method.[37] Once the free thiol concentration is known, then the number of polymer chains that can be immobilized onto the electrode surface via thiol cross-linking can be estimated. DTNB (4 mg) was dissolved into 1 mL of 1× PBS buffer solution of pH 7.2 to prepare the Ellman's reagent. The poly(NIPAM-VP-MAA) powder (10 mg) was also dissolved into 5 mL of 1× PBS buffer solution separately, and then 100 μL of the prepared Ellman's reagent was added to the polymer solution. This solution was stirred for 45 min at room temperature, and then, one aliquot of this solution was taken at regular intervals and diluted with 9 mL of distilled water. The absorbance of these solutions was recorded by UV−vis analysis at 412 nm. Finally, the concentration of free thiol was calculated by the following equation.

$$A = \varepsilon bc \tag{1}$$

where A is the absorbance, ε is the molar extinction coefficient of 2-nitro-5-thiobenzoic acid at 412 nm (14 250 M^{-1} cm^{-1}), b is the length of the cuvette cell (cm), and c is the free thiol concentration (mol L^{-1}).

2.7. Preparation of the Sensor Electrode and Electrochemical Measurements. The gold electrode was cleaned by the following protocol.[38] All electrode potentials are given with respect to the Ag/AgCl reference electrode saturated with 3 M KCl. The gold electrode was first polished with a nylon-based substrate and a mixture of DI and 1 μm diamond suspension (1 μm diamond polish, BASi) for 2 min and then gently rinsed with ethanol for a few seconds. Afterward, the gold electrode was polished again with a fine micro cloth and a 0.05 μm alumina slurry (0.05 μm diamond polish, BASi) to obtain a smooth surface for the gold electrode. Then, further cleaning was carried out by performing the oxidation and reduction reactions in both basic and acidic solutions. The electrochemical cleaning was first performed under a basic solution of 0.5 M NaOH with a potential range of 0.35−1.35 V for typically 300 cycles with a scan rate of 2 V s^{-1}. Then, the gold electrode was polished with a micro cloth and 0.05 μm alumina slurry for 1 min and rinsed with ethanol and DI water, respectively. Afterward, the NaOH-based cleaning was repeated once again for 1000 cycles. Next, electrochemical cleaning was then performed in an acidic solution of 0.5 M H_2SO_4 by applying a potential of 2 V for 5 s and then the potential of −0.35 V for 10 s, respectively. The electrode cleaning was then followed by scanning the potential from 0.35 to 1.5 V, typically for 20 cycles at a scan rate of 4 V s^{-1} and then 20 more cycles at a scan rate of 0.1 V s^{-1} in the same solution. Finally, the gold surface was cleaned by performing the electrochemical oxidation and reduction in a 0.01 M KCl/0.1 M H_2SO_4 in the potential range of 0.2−1.5 V (5 scans at a scan rate of 0.1 V s^{-1}). The prepared electrode was thoroughly rinsed with DI water for a few seconds and kept in DI water before use.

A desired amount of poly(NIPAM-VP-MAA)-*g*-$Os(bpy)_2Cl$ and TCEP (1:1 mass ratio) was dissolved in a 1:1 mixture of 1× PBS:DMF. The surface of a cleaned gold electrode was first dried with a nitrogen gas stream, and then, 10 μL of the prepared polymer solution was dropped onto its surface and kept under vacuum overnight. Prior to performing the sensing experiments, after rinsing the polymer-modified electrode with DI water and $NaClO_4$, at least 15 runs of CV were performed (with each run consisting of 10 cycles) to ensure that a stable CV curve was obtained. The cyclic voltammetry (CV) analysis was performed in the potential range of 0−0.6 V with a scan rate of 100 mV/s in 10 mM $NaClO_4$ solution for all experiments. This step was repeated, until a stable current intensity was achieved. The square-wave voltammetry (SWV) analysis was carried out in the potential range of 0−0.6 V with a pulse height of 50 mV and a pulse width of 300 ms. The electrode was gently rinsed with DI water before the electrochemical analyses were performed, and a fresh electrolyte was used for each experiment. For all sensing experiments, the electrode was exposed to a given concentration of analyte with an incubation time of 1 min before collecting either CV or SWV measurements.

2.8. Sample Preparation for SPR Analysis. *2.8.1. Immobilization of N-mGlu Ligand.* For SPR analysis, an OpenSPR instrument

https://doi.org/10.1021/acsapm.4c00121
ACS Appl. Polym. Mater. 2024, 6, 5630−5641

was used (Nicoya Lifesciences, Kitchener, ON, Canada). For ligand immobilization, amine-functionalized SPR sensor chips (Nicoya Lifesciences Inc.) were used to attach *N*-mGlu to the sensor chip's surface. The carboxyl group of *N*-mGlu was attached to the amine group on the surface of the chip through EDC/NHS chemistry, where PBS buffer (1×, pH 7.2) was used as a running buffer for the ligand immobilization step.

In the ligand immobilization step, 150 μL of 10 mM HCl (pH 2) was first injected at a flow rate of 150 μL/min to clean and activate the amine functional group of the amine chip. *N*-mGlu (20 mg) was dissolved in 300 μL of MES buffer, pH 6. EDC (4.5 mg) and NHS (2.3 mg) were also dissolved in 300 μL of MES buffer, and then, EDC/NHS solution was added to *N*-mGlu solution and stirred for 1 h to activate the carboxylate groups of *N*-mGlu. The immobilization of the *N*-mGlu ligand on the chip surface was subsequently followed using an injection of 150 μL of the prepared *N*-mGlu/EDC/NHS mixture at a flow rate of 20 μL/min. Then, 30 μL of a 2-bromoethanol dissolved into a 1× borate buffer (1 mL) was injected into both channels at a flow rate of 20 μL/min to deactivate the unreacted amine groups of the amine chip. A poly(NIPAM-VP-MAA)-*g*-Os(bpy)$_2$Cl (50 μM) was diluted by a 1,250 ppm BSA solution (prepared in 1× PBS, pH 9) to prepare the dilute polymer solution of 0.5, 1, 3, 5, 7, and 10 μM to be used for studying the polymer/*N*-mGlu binding interactions. A 1250 ppm BSA solution (prepared in 1× PBS, pH 9) was used as a running buffer for this step.

2.8.2. Immobilization of Histamine Ligand. The high-sensitivity carboxylated SPR sensor chip (Nicoya Lifesciences Inc.) was used for immobilizing histamine onto the chip's surface. To clean and activate the carboxyl group, 150 μL of 10 mM HCl was first flown to the chip's surface at a flow rate of 150 μL/min. A mixture of EDC (4.5 mg) and NHS (2.7 mg) dissolved into 300 μL of MES buffer (pH 6) was injected at a flow rate of 20 μL/min. Then, the EDC/NHS coated surface was further functionalized by injecting a histamine solution (35 mM) at a flow rate of 20 μL/min. The intact carboxylic acid groups of the chip were then deactivated by the injection of 150 μL of the blocking solution (Nicoya Lifesciences Inc.). The different concentrations of poly(NIPAM-VP-MAA)-*g*-Os(bpy)$_2$Cl solutions were prepared by following the above protocol, and the same running buffer was used for studying the polymer/histamine binding interaction.

2.9. Characterization. Proton nuclear magnetic resonance spectroscopy (^{1}H NMR) by Bruker 500-MHz ^{1}H NMR instrument and attenuated total reflection (ATR) by a Thermo Nicolet iS10 FTIR with a wavenumber resolution of 0.4 cm^{-1} were used to characterize the chemical structure of the synthesized polymer samples. Thermogravimetric analysis (TGA) (Mettler Toledo) and UV−vis spectroscopy by a PerkinElmer Lambda 800 were used to detect osmium complex in the synthesized polymer samples. For TGA, a desired amount of samples were heated from 25 to 600 °C under an Ar gas atmosphere at a heating rate of 10 °C/min. The molecular weight and polydispersity index (PDI) of the synthesized polymer were determined by gel permeation chromatography (GPC) (Waters Alliance 2695).

3. RESULTS AND DISCUSSION

3.1. Polymer Characterization. ^{1}H NMR analysis was used to identify the chemical structure of the synthesized polymer. As shown in Figure 2, characteristic signals for the protons belonging to the poly(4-vinylpyridine) (PVP) rings are observed at 7 and 8.4 ppm. In addition, the peaks at 1−1.2 ppm and 1.25 ppm are assigned to the protons of the methyl groups of the PNIPAM and poly(methacrylic acid) (PMAA) segments, respectively. The other peaks can be attributed to $CDCl_3$, H_2O, and acetone solvents. The molar ratio of each polymer segment was calculated according to the following equations.

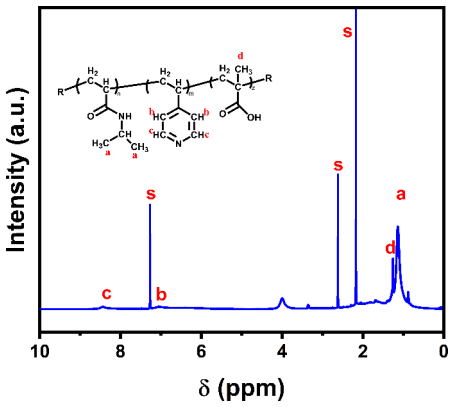

Figure 2. ^{1}H NMR spectra of the synthesized poly(NIPAM-VP-MAA) copolymer.

$$\text{PNIPAM}\ (\%) = \left[\frac{I_a/6}{(I_a/6 + (I_b + I_c)/4 + I_d/3)}\right] \times 100 \quad (2)$$

$$\text{PVP}\ (\%) = \left[\frac{(I_b + I_c)/4}{(I_a/6 + (I_b + I_c)/4 + I_d/3)}\right] \times 100 \quad (3)$$

$$\text{PMAA}\ (\%) = \left[\frac{I_d/3}{(I_a/6 + (I_b + I_c)/4 + I_d/3)}\right] \times 100 \quad (4)$$

Based on the above calculations, the molar ratios of PNIPAM, PVP, and PMAA segments in the poly(NIPAM-VP-MAA) copolymer were determined to be 68.70%, 17.60%, and 13.70%, respectively. Furthermore, the GPC analysis showed that the poly(NIPAM-VP-MAA) copolymer was successfully synthesized by the RAFT polymerization method. The average molecular weight (MW) and the polydispersity index (PDI) of the synthesized copolymer as analyzed by GPC were 6258 g mol^{-1} and 1.49, respectively (Figure S1 in Supporting Information). Although there may be other possible methods to estimate the MW of the polymers, the GPC technique appears to be the most reliable and accurate method to measure this parameter. With GPC, in addition to MW, one can also obtain other information about the polymers such as number-average molecular weight (M_n) and PDI among others.

Fourier-transform infrared (FTIR) analysis was also carried out as further evidence to confirm the successful synthesis of poly(NIPAM-VP-MAA) and Os(bpy)$_2$Cl$_2$, and the grafting of Os(bpy)$_2$Cl$_2$ to the polymer backbone to form poly(NIPAM-VP-MAA)-*g*-Os(bpy)$_2$Cl (Figure 3A). For the poly(NIPAM-VP-MAA) sample, a group of peaks that appears near 1,400 cm^{-1} is attributed to the aromatic rings of vinylpyridine. A characteristic peak assigned to C═O group is observed at 1560 cm^{-1} and 1720 cm^{-1} for PNIPAM and PMAA, respectively. The main index peak associated with the pyridine ring (−C═N−C−) of the Os(bpy)$_2$Cl$_2$ complex sample is shown at 3400 cm^{-1}.

For the polymer and the modified polymer samples, the peaks belonging to the aliphatic C−H bonds have appeared around 2850−2950 cm^{-1}, confirming the presence of polymer sample in the poly(NIPAM-VP-MAA)-*g*-Os(bpy)$_2$Cl. In addition, the peaks related to carbonyl groups of PNIPAM and PMAA (C═O) were observed in the range of 1500−1700 cm^{-1}. For the poly(NIPAM-VP-MAA)-*g*-Os(bpy)$_2$Cl sample, a

https://doi.org/10.1021/acsapm.4c00121
ACS Appl. Polym. Mater. 2024, 6, 5630−5641

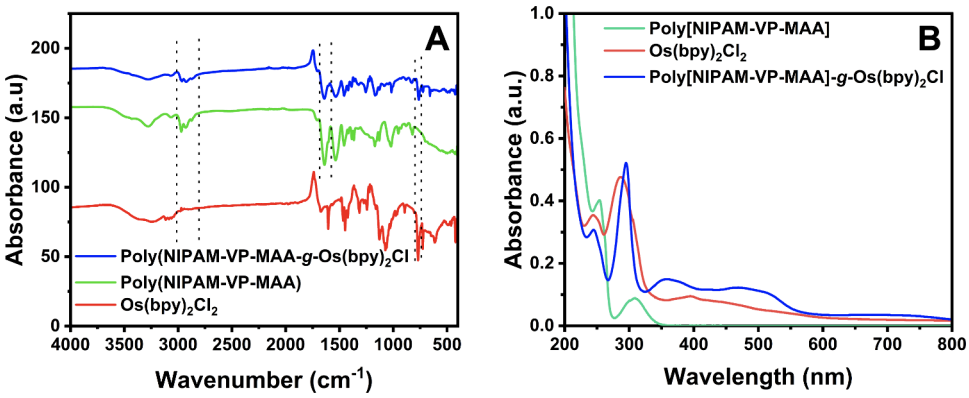

Figure 3. Characterizing the molecular compositions of the stimuli-responsive polymer, poly(NIPAM-VP-MAA), the osmium complex, $Os(bpy)_2Cl_2$, and the stimuli-responsive polymer labeled with osmium complexes, poly(NIPAM-VP-MAA)-*g*-$Os(bpy)_2Cl$, using (A) FTIR and (B) UV−vis spectra.

new peak that appeared at 750 cm^{-1} can be attributed to the C−C bond of the pyridine ring. These peaks manifested evidence that the $Os(bpy)_2Cl_2$ complex has been successfully grafted to the poly(NIPAM-VP-MAA) backbone through PVP segments. One important note is that when $Os(bpy)_2Cl_2$ reacts with PVP to form a bond, one Cl is replaced by the vinylpyridine ring. Thus, after grafting to the polymer, the osmium complex loses one Cl to form poly(NIPAM-VP-MAA)-*g*-$Os(bpy)_2Cl$.

Figure 3B depicts the UV−vis spectra of the samples dissolved in 1× PBS. Both the $Os(bpy)_2Cl_2$ and osmium-grafted polymer displayed a strong and sharp peak at around 290 nm, while the unmodified polymer sample does not show this peak at this particular wavelength. These absorbance peaks originate from osmium and reveal the presence of the osmium complex in the synthesized poly(NIPAM-VP-MAA)-*g*-Os-$(bpy)_2Cl$ copolymer sample. The electrochemical characterization of these samples was also performed to reveal the electroactivity of the synthesized osmium complex and the osmium-grafted polymer (Figure S3 in the Supporting Information) prior to sensor development. The osmium complex displayed an oxidation/reduction peak around 0 V vs Ag/AgCl. In contrast, the electrochemical behavior of this complex, when grafted to a polymer, exhibits oxidation/reduction peaks appearing at a significantly higher potential voltage at 0.27 V. This result is in agreement with the previous reporting that the polymer backbone can affect the redox behavior of the redox tag, which is incorporated as a side chain or an adjacent group in the polymer chains.[20] The polymer chains can affect kinetic aspects such as reducing diffusional access and attractive/repulsive interactions, thereby modifying the redox behavior of the electroactive species.[20,39] The polymer backbone property, such as polarity, can also be affected by electroactive species, especially those that show significant electrostatic charge differences in the oxidation/reduction states.[20] The attached polymer on the electrode surface can also alter the electron tunneling and transport on the electrode surface, which radically changes the electrochemical behavior of the attached redox labels when compared to their untethered or ungrafted state. However, the degree to which such changes in their electrochemical properties are exhibited is highly dependent upon a few key factors, including the polymer chain length (or the molecular weight) and polymer crowding on the electrode surface. As shown in Figure S3, the electrochemical behavior of the poly(NIPAM-VP-MAA)-*g*-$Os(bpy)_2Cl$ attached to the electrode shows similar trend as the polymer dispersed in solution. This suggests that the polymer density and molecular weight are appropriate such that the polymers are well-dispersed without any significant crowding or entanglement. This matching electrochemical behavior between polymer-grafted electrode and bare electrode immersed in polymer-dispersed solution would not be observed in the case of high molecular weight polymers even in low polymer density (i.e., concentration) due to entanglements caused by long polymer chain lengths. Furthermore, the electrode sensors fabricated following the protocol mentioned above displayed good electrochemical activity and stability over time. The electrochemical behavior of the fabricated electrode was investigated by attaching the synthesized electrode onto the gold electrode surface through the thiol chemistry (Au−S bond).[1] Optimization of the amount of TCEP required to convert the disulfide bond S−S to the S−H group, which comes from the RAFT agent used for polymer synthesis, was carried out by UV−vis analysis (Figure S4 in the Supporting Information). The amount of free thiol group measured by Ellman's assay was found to be 23 μM using eq 1 in section 2.6 and thiol absorption spectra (Figure S4b in Supporting Information).

Thermogravimetric analysis (TGA) was also carried out as supplementary analyses to provide evidence of the grafting of $Os(bpy)_2Cl_2$ to the polymer backbone (Figure S2 in Supporting Information). The TGA thermograms indicate that the synthesized polymer and the polymer modified with the osmium complex demonstrated good thermal stability up to 250 °C. For both samples, the weight losses observed below 250 °C are attributed to the evaporation of the residual solvent trapped in the samples. The higher char content of poly(NIPAM-VP-MAA)-*g*-$Os(bpy)_2Cl$ compared to poly-(NIPAM-VP-MAA) confirms that grafting of the amorphous compound to the polymer backbone was successful. Furthermore, the poly(NIPAM-VP-MAA)-*g*-$Os(bpy)_2Cl$ shows a char content of around 45 %w/w, which is much larger than that of the poly(NIPAM-VP-MAA). The differences between the char content of the osmium-grafted polymer and that of the polymer can be attributed to the char from the $Os(bpy)_2Cl_2$ complexes.

3.2. Optimization of the Polymer Surface Coverage of the Electrode. Different concentrations of poly(NIPAM-VP-MAA)-*g*-$Os(bpy)_2Cl$ solution were investigated to determine the optimum surface coverage (i.e., density) of the

https://doi.org/10.1021/acsapm.4c00121
ACS Appl. Polym. Mater. 2024, 6, 5630−5641

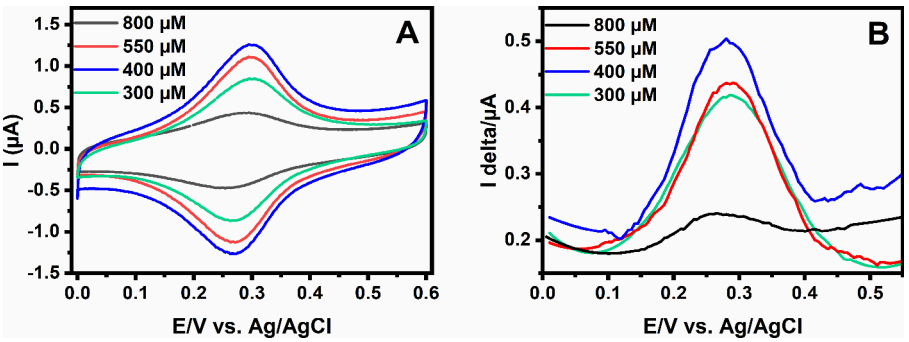

Figure 4. CV (A) and SWV (B) of the modified electrode with different concentrations of poly(NIPAM-VP-MAA)-*g*-Os(bpy)$_2$Cl.

polymer on the electrode to achieve high-sensitivity detection. To accomplish this, the signal intensity was optimized by changing the density of the polymer attached to the electrode. The electrodes were fabricated following the protocol described in section 2.6, and all CV and SWV measurements were recorded after attaining a stable current, which was obtained by repeating at least 15 runs in this case. It should be noted that the fabricated electrode was gently rinsed with DI water to remove the unattached polymer chains and unreacted Os(bpy)$_2$Cl$_2$ from the gold electrode surface before each run. As shown in Figure 4, both anodic and cathodic currents have gradually risen as polymer concentrations increased to 550 μM.

In contrast, significant signal suppression was observed at the highest concentration (800 μM) investigated. This finding is consistent with the results reported previously.[39] The high density of the polymer chain on the electrode surface can diminish electron diffusion and transport, thereby suppressing signaling. Since the electron transfer rate can also be affected by the conformational change of the polymer, the attached polymer chains are likely to be pushed away from the electrode surface densely packed and crowded with polymers due to the electrostatic repulsion among them. In other words, the conformation of the polymer chains can facilitate or hinder electrons from reaching the electrode surface. Although it appears from Figure 4 that the 400 μM polymer concentration has a higher peak compared to the 550 μM concentration, after baseline subtraction, the 550 μM concentration shows a slightly higher current peak than the 400 μM concentration (Figure S7 in Supporting Information). From these CV and SWV results, 550 μM poly(NIPAM-VP-MAA)-*g*-Os(bpy)$_2$Cl solution was chosen as the optimum polymer concentration for preparing the biosensor and was used for the subsequent procedures.

It is also possible to estimate the number of polymers attached to the electrode by counting the total charge passed through the electrode during the forward sweep of CV (Figure S8 in the Supporting Information) and by calculating the average number of osmium complexes per polymer chain. Based on our calculation, we estimate the polymer density to be 7.8×10^{10} polymers/mm^2.

3.3. The Effects of Ions on the Polymer's Conformation. Since the proposed sensing mechanisms are dependent upon the conformational changes of the stimuli-responsive polymers, it is important to discuss how various types of anions in the solution interact with the polymer. The salt effect on the stability of the solutes in an aqueous solution is known as the Hofmeister effect, which is more pronounced for anions than cations.[40−42] The Hofmeister effect is a result of several ionic properties, such as the partition coefficient, hydration energetics, polarizability, and size, which can vary from one ion to another. In other words, this effect is ion-specific and heavily dependent on the ingredients in the buffer solution. Based on the Hofmeister phenomenon, the anions are categorized into two main groups: strongly hydrated (or kosmotropic) anions and weakly hydrated (or chaotropic) anions.[40−42] The following lists the anions in the order of their hydration strength, where CO_3^{2-} is the most kosmotropic and SCN^- is the most chaotropic. Also, the anions listed to the left of Cl^- are considered to be kosmotropes, while the anions to the right of Cl^- are considered to be chaotropes.[40−42]

$$CO_3^{2-} > SO_4^{2-} > S_2O_3^{2-} > H_2PO_4^- > F^- > Cl^- > Br^- \approx NO_3^- > I^- > ClO_4^- > SCN^-$$

This list reveals the ion−water interaction in a solution. The strongly hydrated anions can make a more robust ion−water interaction than a water−water interaction, while the weakly hydrated anions show the opposite behavior.

Previous studies have suggested that the Hofmeister series can tune the conformation change of a thermal-responsive polymer through anion interaction with the polymer and the polymer's adjacent hydration shell (Figure S5 in Supporting Information). It has been reported that kosmotropic anions decrease the stability of PNIPAM in a solution and its LCST due to the competition of these anions with polymer for hydration.[43−45] In addition, this instability is caused by the repelling of these anions from the PNIPAM backbone and its isopropyl group (salting-out) due to the increase of the surface tension of these polymer regions as a result of polymer hydration disrupted by the anions.[44] In contrast, the chaotropic anions tend to bind to the N−H group of this polymer (salting-in) and enhance the polymer stability in the solution, thereby raising its LCST in a nonlinear manner.[44] Thus, these anions can be accumulated at the polymer surface due to the absence of bulk hydration of the polymer through ion-induced electrostatic interaction with the N−H moieties with a partial positive charge.[43,44]

Regarding the choice of electrolyte to be used for sensing applications, sodium perchlorate ($NaClO_4$) solution was selected since ClO_4^- is a highly chaotropic anion, and thus, the polymers are expected to exhibit stable conformations in this environment. Furthermore, a larger zeta potential value for the polymer dissolved in $NaClO_4$ solution compared to that in other solvents reveals the effective stabilization of polymer chains through a repulsive electrostatic force in the $NaClO_4$ solution (Table S1 in Supporting Information). The polymer modified with osmium complex also shows a similar trend with

https://doi.org/10.1021/acsapm.4c00121
ACS Appl. Polym. Mater. 2024, 6, 5630−5641

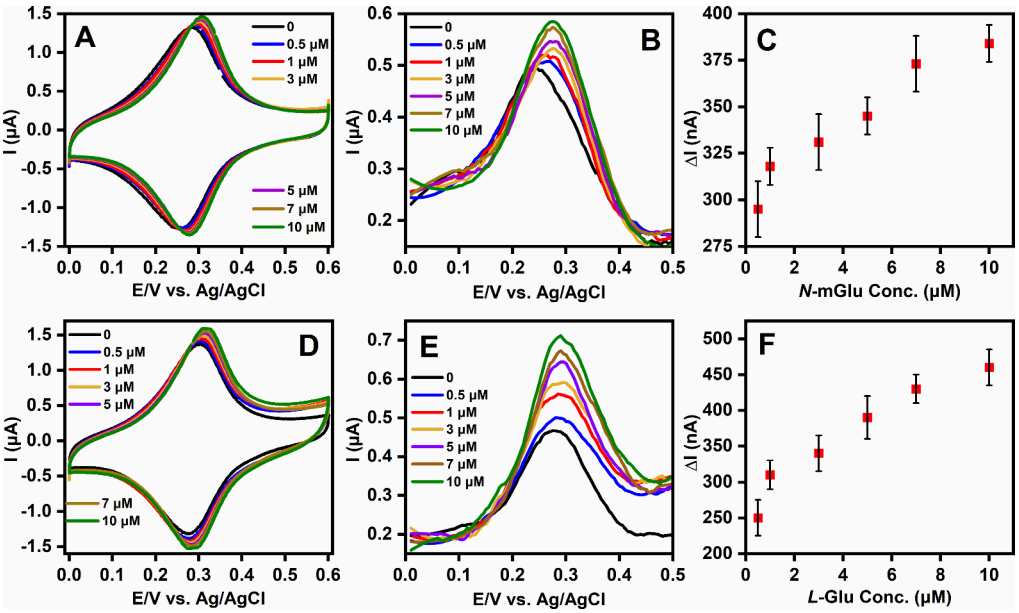

Figure 5. Electrochemical sensing results were obtained using the polymer-modified electrode. CV (A) and SWV (B) plots when the sensor electrode was exposed to 0.5−10 μM of *N*-mGlu; (C) calibration curve for *N*-mGlu detection using the peak current values from SWV; CV (D) and SWV (E) plots when the sensor electrode was exposed to 0.5−10 μM of *L*-Glu; (F) calibration curve for *L*-Glu detection using the peak current values from SWV. The error bars represent 1 standard deviation (n = 3). All experiments were performed with a 10 mM $NaClO_4$ electrolyte.

almost identical zeta potential values to the unmodified polymer in the $NaClO_4$ solution, indicating a negligible impact on the polymer conformation due to the addition of osmium complexes to the polymer.

3.4. Electrochemical Sensing of Glutamate. Since *N*-mGlu, an organic soluble derivative of glutamate, was used as a template molecule during the polymer synthesis instead of *L*-Glu due to the insolubility of *L*-Glu in the dioxane solvent to synthesize the designed polymer, the performance of the developed polymer-based biosensor was investigated by exposing different concentrations of both *N*-mGlu and *L*-Glu in $NaClO_4$ electrolytes. As shown in Figure 5, the polymer-based biosensor shows a similar trend when exposed to bacterial *N*-mGlu and *L*-Glu molecules in 10 mM $NaClO_4$ solution. The peak intensity or current was increased as the *N*-mGlu and *L*-Glu concentrations were raised, and the oxidation potential shifted slightly toward positive values. This behavior verifies the polymer's capability of conformational change from extended (target unbound) to folded (target bound) shape due to the absence and presence of the target molecules, respectively. It is interesting to note that although the polymers are templated with *N*-mGlu and therefore are expected to exhibit the highest sensitivity in *N*-mGlu detection, *L*-Glu detection shows better sensitivity. One possible explanation is that changes in the pH level caused by the addition of the analyte in the buffer may impact the sensor's sensitivity. When *N*-mGlu and *L*-Glu are dissolved in solutions, because of the differences in the ammonium groups, these two solutions result in different pH levels (if the same amounts were dissolved) with the *L*-Glu solution being slightly more acidic than the *N*-mGlu solution. Since our polymer is pH-sensitive, this would yield slight differences in the polymer conformation and therefore differences in sensor responses. The presence of *L*-Glu in the buffer shifts the pH in a more acidic direction that causes the polymers to undergo a greater conformation change than they would in a buffer with *N*-mGlu. The limit of detection (LOD) of this sensor can be calculated following the formula: LOD = 3.3 × σ/S, where σ is the standard deviation of the response and S is the slope of the calibration curve. We found that the LOD for the Glu biosensor is approximately 0.3 μM.

In a related study, Zajforoushan et al. studied the effects of chaotropic and kosmotropic anions on the stability and conformation of PNIPAM in bulk solution and at the gold-aqueous interface.[43] Based on the quartz crystal microbalance with dissipation (QCM-D) measurement, the attached soft polymeric film illustrates a high dissipation (damping) value, indicating deforming polymeric film during oscillation. In contrast, the attached rigid polymeric film shows no significant deformation, exhibiting a small damping factor. Moreover, a lower collapse temperature was found for the polymers confined at the solid−liquid interface than that in bulk solution.[43] Based on Zajforoushan's finding, the physically adsorbed PNIPAM film on the gold surface has shown the partially collapsed film with more rigidity by changing the solvent from water to the NaF solution (water containing the kosmotropic anion (F^-)),[43] while an opposite behavior has been reported for PNIPAM film in contact with the water containing chaotropic anion (SCN^{-1}).[43] The swelling of the PNIPAM film in the presence of a chaotropic anion can imply the strong affinity of this anion to accumulate at hydrophobic groups of PNIPAM (or the direct anion-PNIPAM interactions), thereby diminishing the hydrophobic hydration of polymer, which results in polymer chain stability.

Recognizing the "signal-on" bahavior of the sensor when it is exposed to either *N*-mGlu or *L*-Glu in $NaClO_4$ solution, our findings strongly confirm the importance of polymer chain conformation on its sensing performance which is controlled by the determining factors such as solvent quality and its additives. The PNIPAM-based polymer chains are open and unfolded in $NaClO_4$ solution, thereby facilitating polymer−analyte interaction and polymer conformational change. A

https://doi.org/10.1021/acsapm.4c00121
ACS Appl. Polym. Mater. 2024, 6, 5630−5641

highly chaotropic anions (such as perchlorate ions) tend to bind to the NH groups of the polymer promoting stability and raising its LCST. This leads to the polymer changing its conformation from a tightly collapsed and folded state to an open and unfolded state. Also, from the literature,[43−45] the zeta potential in the range of −30 to +30 indicates that the polymer has low stability and therefore is in a collapsed morphology with low solubility. Conversely, the zeta potential outside of this range indicates high stability which means the polymer has a semiopen to open morphology with high solubility. Generally, when the polymer conformation is in the swelled and stretched state, a high detection performance (in terms of both sensitivity and selectivity) is observed for our polymer-based biosensors, regardless of whether the receptor-analyte interaction is repulsive (signal-off) or attractive (signal-on).

Regarding the choice of buffer solution, since neurochemicals are usually measured in the brain region, our sensor's ultimate sample environment would be the cerebrospinal fluid (CSF) for in vivo measurements and artificial CSF (ACSF) for ex vivo and in vitro measurements. Due to the Hofmeister effect, buffers that contain high concentrations of carbonate and phosphate ions generally are not compatible with the proposed polymer formula as the polymers tend to collapse into a closed form in those environments. However, since our polymer is also salt sensitive, the adverse effects of carbonate and phosphate ions can be minimized by utilizing a mixture of various salts to counter the effects of kosmotropic anions. In our recent preliminary studies, we have found that oxygen-saturated artificial cerebrospinal fluid (ACSF) provides an excellent environment for our templated polymers to not only bind with the target molecules but also undergo a conformation change upon target recognition, which is a promising sign that the proposed sensing platform can detect neurochemicals in a real physiological environment.

3.5. Target Selectivity Characterization. The target selectivity of the fabricated electrochemical biosensor was then tested with different concentrations of other potential interfering species, namely, histamine (HIS), serotonin (5-HT), dopamine (DA), and gamma aminobutyric acid (GABA). As shown in the CV results in Figure 6, no obvious response was observed for the serotonin and GABA molecules. The current intensity has mainly remained constant in the different concentrations of these molecules, while dopamine resulted in a slight increase in the sensing current (Figure 6B). Another interesting finding is that the sensing response of this biosensor was converted from "signal-on" to "signal-off" upon exposure to the HIS. Figure 6D and Figure 6E demonstrate a gradual suppression of current with a distinct potential shift toward the negative potential with an increasing concentration of HIS. A decrease in the sensing response reveals that histamine prevents polymer chain folding, thereby hindering electron transfer between the redox tag and the electrode surface. In fact, the designed polymer can exhibit varying polymer chain conformations based on the electrostatic self-assembly induced by nontarget molecules. The sensor's selectivity against a potential interfering species will highly depend on the similarities in its molecular structure to the target molecule. Indeed, when the sensor was exposed to molecules that closely resemble glutamate, such as aspartate, a significant sensor response was observed (approximately 60−70% of sensor response to *L*-Glu of the same concentration). If the sensor is to be used in real physiological conditions, such as a brain tissue environment, one effective strategy to minimize false positive responses would be to apply pharmacological techniques by introducing drugs that block the release of potential interfering species. Therefore, it is worth noting that the experimental setup and the sensor's specific location within the tissue sample will largely determine the selectivity requirements and the interfering species of concern that need to be addressed in order to achieve a successful measurement of the analyte.

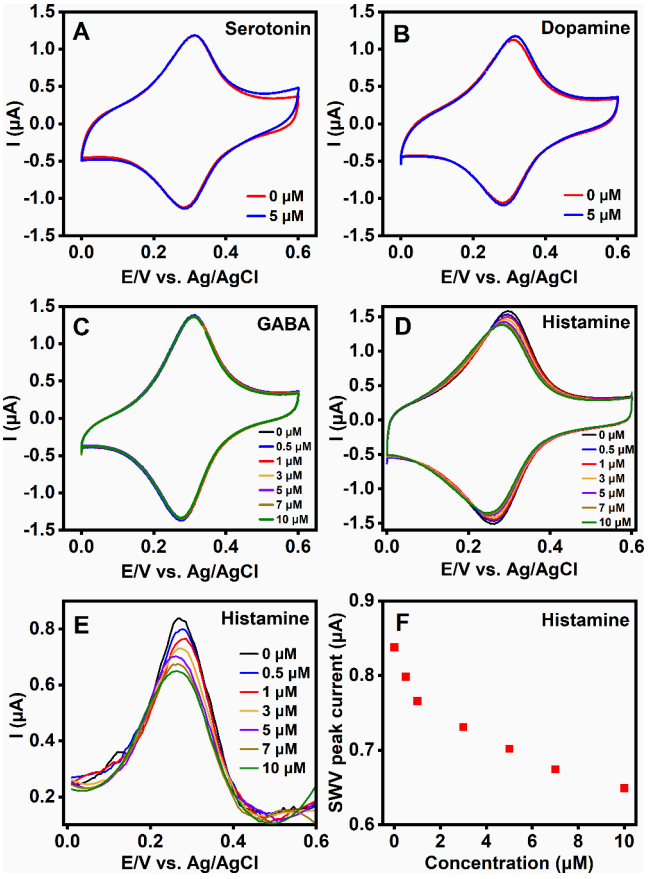

Figure 6. Characterization of the chemical selectivity for the developed biosensor. The cyclic voltammetry (CV) responses of the polymer-modified electrode under exposure to serotonin (A), dopamine (B), GABA (C), and histamine (D). The square-wave voltammetry (SWV) responses (E) and its calibration curve (F) for histamine detection show the "signal-off" behavior of the biosensor. The electrolyte used was 10 mM $NaClO_4$.

3.6. Effects of Polymer Chain Length on the Sensor Response. It is reasonable to anticipate that the polymer chain length (i.e., the molecular weight) will play a major role in the sensor's response. As the polymer chain length increases, the sensor response will become more sensitive due to the greater change in the conformation and therefore the greater displacement of the redox-active labels. However, the sensor's response time may increase due to the potential interchain interactions and the "tangling" of the polymers which may delay the target-induced conformation change. On the other hand, if the polymer length is shorter, a faster response may be expected due to reduced interchain interaction and the target's easy access to the binding sites. However, the sensitivity may be reduced due to the polymer's shorter actuation distance. Therefore, optimizing the chain length is required for the practical applications of this sensor platform.

https://doi.org/10.1021/acsapm.4c00121
ACS Appl. Polym. Mater. 2024, 6, 5630−5641

3.7. Effects of Redox Labels (Osmium Complexes) on the Sensitivity of Target Detection. One of the advantages of the proposed redox-labeled templated polymers is that it allows for the inclusion of multiple numbers of redox reporters to each polymer chain, thereby amplifying the voltammetric responses as opposed to having only a single redox tag per target receptor probe (which is typically the case for redox-tagged aptamers). However, the locations of these redox reporters in the polymer chain play a critical role in generating a highly sensitive detection response. The polymers synthesized in this work consist of randomized sequences of NIPAM, MAA, and VP and since the osmium complexes are bound to VP, the location of the redox tags are randomly distributed along the polymer chain. For maximum sensitivity in sensor responses, it would be preferential to attach the osmium complexes near the end of the polymer chain opposite the RAFT agent. In this way, when the polymers are attached to the electrode, the redox labels are the farthest from the electrode, assuming that the polymers are in an open and linear morphology. As the target molecules bind with the polymers, causing them to fold, a highly sensitive voltammetry response could be observed.

3.8. Sensor Regeneration Capability. After exposure to each concentration of *N*-mGlu, *L*-Glu, and HIS, the regeneration capability of the prepared electrode biosensor was investigated by washing the electrode in a bath of DI water with gentle agitation and then inserting it into 10 mM $NaClO_4$ for 10 min followed by running a CV. Since the polymers are securely attached to the gold surface via a strong thiol bond, gently rinsing the electrode in DI water is not expected to cause any removal of the polymers from the electrode surface. After rinsing with DI water, the polymer conformation may have been altered, as DI water does not contain any chaotropic anions needed to restore the polymer conformation into a stable state. Therefore, the electrode was immersed in $NaClO_4$ solution to ensure that the polymer conformation is returned to its stable partially open morphology before reusing. The biosensor exhibited excellent regeneration behavior (Figure S7 in Supporting Information) when the electrode was exposed to 0.5−10 μM of either *N*-mGlu, *L*-Glu, or HIS, as the sensor was able to fully recover the initial CV curve after rinsing with DI water and keeping in the $NaClO_4$ solution. This demonstrates the reusability and continuous monitoring capabilities of the developed sensor platform. The target recognition event that occurs between the binding sites in the templated polymers and the target molecules is reversible with the forward binding (i.e., association) rate and the reverse unbinding (i.e., dissociation) rate reaching a certain equilibrium, similar to the aptamer's target binding mechanism. Due to this reversibility in target-receptor interaction, DI water is sufficient to disrupt the bond between the target and the polymer to achieve regeneration of the polymers. Moreover, DI water, having little ionic content compared to $NaClO_4$, is likely to cause mild conformation changes in the polymer which may further help free the bound target molecules from the binding sites of the templated polymers. The reversibility of our polymer's binding kinetics suggests that the proposed biosensing platform may be able to achieve continuous monitoring of the analyte without the need for an active regeneration of the sensor.

Upon oxidation, the net charge of the polymer chain is expected to be partially positive due to the electron loss of the osmium metal. The charge variation of the polymer chains during electrochemical measurement improves the attractive interaction between the polymer chain and anion analytes (glutamate derivatives). However, this charge variation can give rise to a repulsive force between the polymer chains and the cationic analytes, such as HIS, thereby unfolding the polymer chains upon cationic analyte exposure. In addition, no significant variation in the sensing response of the designed biosensor was observed due to a strong ion pair that exists between the positively charged quaternary ammonium group and its counterion (chloride anion). This phenomenon can interfere with the effective interaction between the polymer and the target analyte and cause a certain degree of polymer chain folding in the case of exposure to DA. Another possibility is that the oxidation of the electroactive species (such as DA and 5-HT) may interfere with the redox response of the osmium redox label of the polymer.

3.9. SPR Analysis. The SPR analysis was carried out to validate the polymer's binding affinity with *N*-mGlu, and HIS ligands. For this purpose, *N*-mGlu and HIS ligands were immobilized on the amine-coated and carboxyl-coated chips, respectively, through amide linkages, and the unreacted functional groups were deactivated by a blocking agent. The SPR sensorgram showed a more significant response in the reference (buffer only) channel than in the sample (polymer in buffer) channel when PBS buffer was used to prepare both the polymer solution and the running buffer, indicating that a strong interaction exists between the polymer and the unreacted amine and carboxylic acid groups on the chip surface (i.e., nonspecific bonding). Various strategies were applied to minimize the nonspecific binding on the surface of the SPR chip, including changing the pH and adding additives such as salt, surfactants, and BSA (bovine serum albumin). The association and dissociation kinetics for the poly(NIPAM-VP-MAA) and poly(NIPAM-VP-MAA)-*g*-Os(bpy)$_2$Cl when exposed to SPR chip functionalized with *N*-mGlu are shown in Figure 7A−D. The concentration dependent calibration curves shown on the right column of Figure 7 are obtained using the "Affinity/EC50" curve-fitting model in TraceDrawer software (Ridgeview Instruments, Uppsala, Sweden) based on the SPR sensorgrams. It is worth mentioning that a significant amount of nonspecific adsorption of polymers occurs in addition to the specific binding between the polymers and the target molecules on the SPR chip's surface. As a result, the SPR response appears to be larger than expected. However, applying the proper curve-fitting model, the calibration curves that follow the Langmuir adsorption model are obtained giving a more accurate representation of the equilibrium affinity between the polymer and the target during the association phase.

Upon flowing the polymer solution, the polymer−analyte interaction is expected to lead to a measurable change in the refractive index near the sensor surface. From 25 to 250 s in Figure 7A,C, the *N*-mGlu pre-immobilized surface was exposed to a solution of different concentrations of the polymer to observe the polymer−analyte binding (association phase). After this period, the flowing solution was replaced with PBS buffer containing BSA (running buffer) to induce target release from the chip's surface (dissociation phase). From the calibration curves in Figure 7B,D, the polymer without an osmium redox tag (i.e., poly(NIPAM-VP-MAA)) exhibits a higher binding affinity than the redox-labeled polymer (i.e., poly(NIPAM-VP-MAA)-*g*-Os(bpy)$_2$Cl). This result reveals that the presence of the osmium complex on the polymer

https://doi.org/10.1021/acsapm.4c00121
ACS Appl. Polym. Mater. 2024, 6, 5630−5641

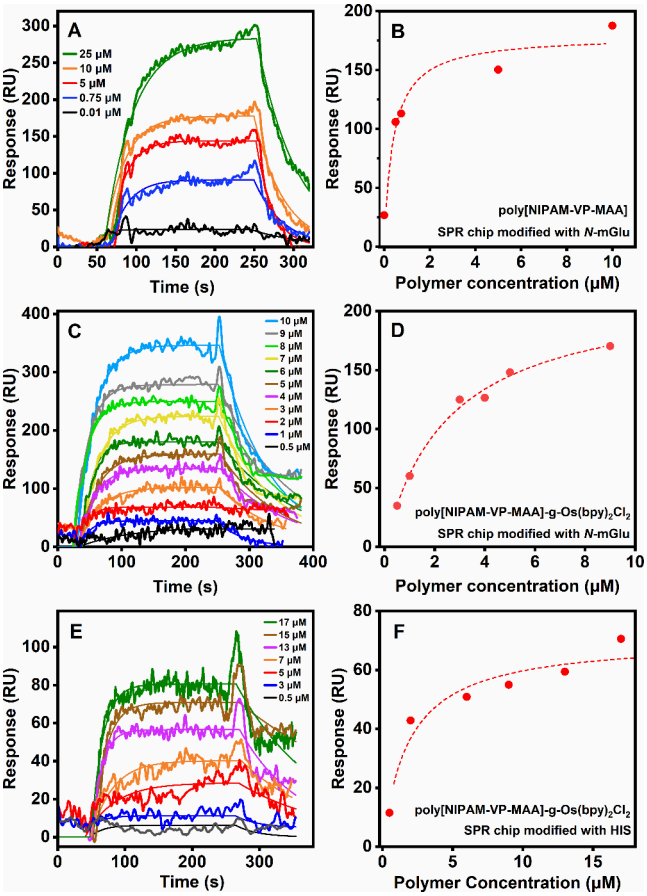

Figure 7. Characterization of the binding kinetics of polymer-based target receptors templated with *N*-mGlu. The figure shows the real-time association/dissociation curves and the corresponding equilibrium binding affinity plot for poly(NIPAM-VP-MAA) with SPR chip functionalized with *N*-mGlu (A, B); poly(NIPAM-VP-MAA)-*g*-$Os(bpy)_2Cl_2$ with SPR chip functionalized with *N*-mGlu (C, D); and poly(NIPAM-VP-MAA)-*g*-$Os(bpy)_2Cl_2$ with SPR chip functionalized with histamine (E, F). The calibration curves were obtained based on the "Affinity/EC50" model of curve fitting of the SPR sensorgrams.

has a significant impact on the polymer−analyte binding affinity.

Furthermore, the equilibrium dissociation constant (K_D), which represents the concentration at which half of the ligands binding sites on the polymer is occupied, was evaluated using a one-to-one fitting model (Figure 7A,C) and a steady-state affinity model (Figure 7B,D) in the TraceDrawer software . As shown in the polymer/ligand binding assay (Figure 7B,D), the K_D of polymer/*N*-mGlu binding was estimated to be 390 nM and 2.40 μM for the redox-free polymer and the osmium-grafted polymer, respectively. Moreover, the SPR demonstrated a similar association/dissociation behavior as the polymer was flown over the histamine (His)-immobilized SPR chip, confirming the affinity and specific binding of His to the synthesized polymer (Figure 7E,F). From the steady-state affinity fitting model, the K_D of the osmium-grafted polymer/His binding was estimated to be 1.54 μM. It is important to note that while SPR provides valuable information in terms of the affinity between the polymer and the target as well as the real-time binding kinetics, it is not able to confirm the type of conformational changes (whether folding or unfolding) that the polymer undergoes as it binds to the analyte. Therefore, similar parameters for binding kinetics were obtained for both *N*-mGlu and His even though the polymer exhibits signal-on (folding) and signal-off (unfolding) behaviors, respectively.

4. CONCLUSION

A novel stimuli-responsive polymer-based electrochemical biosensor was developed to determine glutamate and histamine neurotransmitters. To achieve this, a poly(NIPAM-VP-MAA) hybrid labeled with the osmium complex as a redox tag was synthesized by RFAT polymerization and utilized as a polymeric target recognition element to implement an electrochemical biosensor. ^{1}H NMR, FTIR, UV−vis, TGA, and electrochemical analyses confirmed the successful synthesis of the designed poly(NIPAM-VP-MAA)-*g*-$Os(bpy)_2Cl$ as a synthetic receptor. The CV and SWV results revealed a concentration-dependent behavior for the fabricated biosensor to glutamate and histamine exposure, demonstrating the polymer's capability as a selective target receptor and a label-free electrochemical biosensor. The electrochemical analysis reveals that the designed biosensor exhibited a "signal-on" mechanism when detecting glutamate (i.e., polymer folds when target is bound) while a "signal-off" mechanism was observed when detecting histamine (i.e., polymer extends when target is bound). The developed sensor also exhibited excellent target selectivity due to the polymers being templated with analyte molecules, and no significant sensor response was observed when exposed against DA, 5-HT, and GABA. The SPR technique was further utilized to validate the electrochemical results and binding affinity between the polymer-based receptor and the analyte (i.e., glutamate or histamine). Furthermore, the SPR results indicate that polymers without the osmium-based redox label possess stronger affinity to glutamate compared to the polymers labeled with osmium complex. Finally, the sensor demonstrated excellent regeneration capability, suggesting that the proposed sensing technology has a potential to be used in real-time analyte monitoring applications.

■ ASSOCIATED CONTENT

Supporting Information

The Supporting Information is available free of charge at https://pubs.acs.org/doi/10.1021/acsapm.4c00121.

Gas permeation chromatography (GPC) curve of the synthesized poly(NIPAM-VP-MAA) copolymer (Figure S1); thermogravimetric analysis (TGA) curves of poly(NIPAM-VP-MAA) and poly(NIPAM-VP-MAA)-*g*-$Os(bpy)_2Cl$ copolymer samples (Figure S2); CV and SWV curves of $Os(bpy)_2Cl_2$, poly(NIPAM-VP-MAA)-*g*-$Os(bpy)_2Cl$, and gold electrode modified with poly(NIPAM-VP-MAA)-*g*-$Os(bpy)_2Cl$ (Figure S3); UV−vis spectra of the thiolated poly(NIPAM-VP-MAA) in the presence of TCEP and Ellman reagent (Figure S4); schematic illustration of the Hofmeister effects (Figure S5); ζ potentials of the polymers (Table S1); sensor regeneration studies (Figure S6); background subtracted SWV curves of polymer-modified electrodes (Figure S7); polymer density estimation on electrode surface (Figure S8) (PDF)

https://doi.org/10.1021/acsapm.4c00121
ACS Appl. Polym. Mater. 2024, 6, 5630−5641

AUTHOR INFORMATION

Corresponding Author

Edward Song − *Department of Electrical & Computer Engineering, University of New Hampshire, Durham, New Hampshire 03824, United States;* orcid.org/0000-0003-1702-4044; Email: Edward.Song@unh.edu

Authors

Leila Ahmadian-Alam − *Department of Electrical & Computer Engineering, University of New Hampshire, Durham, New Hampshire 03824, United States*

Arturo Andrade − *Department of Neuroscience and Robert J. & Nancy D. Carney Institute for Brain Science, Brown University, Providence, Rhode Island 02912, United States*

Complete contact information is available at: https://pubs.acs.org/10.1021/acsapm.4c00121

Funding

This research was funded by the National Institute of Biomedical Imaging and Bioengineering (NIBIB, Award 1R21EB031433), the National Science Foundation (NSF, Award 1847152), the National Institute of General Medical Sciences (NIGMS, Award P20GM113131), and the National Institute of Mental Health (NIMH, Award R01MH124811).

Notes

The authors declare no competing financial interest.

ACKNOWLEDGMENTS

The authors would like to acknowledge Patricia Stone and John Wilderman from the University Instrumentation Center (UIC) at the University of New Hampshire (UNH) for their assistances in the use of NMR and FTIR; Darcy Silver (College of Engineering and Physical Sciences, Chemical Engineering, UNH) for her assistance in the use of TGA and UV−vis; Prof. Jeffrey Halpern (Chemical Engineering, UNH) for the use of DLS, Wendy Gavin (Core Research Facilities, University of Massachusetts Lowell) for her assistance in performing GPC and analyzing the results. The use of SPR was supported by the UNH Center for Integrated Biomedical and Bioengineering Research (CIBBR) through a grant from the National Institute of General Medical Sciences (NIGMS).

REFERENCES

(1) Ahmad, H. M. N.; Dutta, G.; Csoros, J.; Si, B.; Yang, R.; Halpern, J. M.; Seitz, W. R.; Song, E. Stimuli-Responsive Templated Polymer as a Target Receptor for a Conformation-Based Electrochemical Sensing Platform. *ACS Appl. Polym. Mater.* **2021**, *3* (1), 329−341.

(2) Grenier, C.; Timberman, A.; Yang, R.; Csoros, J.; Papantones, A.; Deravi, L.; Seitz, W. Rapid, High Affinity Binding by a Fluorescein Templated Copolymer Combining Covalent, Hydrophobic, and Acid−Base Noncovalent Crosslinks. *Sensors* **2018**, *18* (5), 1330.

(3) Watanabe, M.; Akahoshi, T.; Tabata, Y.; Nakayama, D. Molecular Specific Swelling Change of Hydrogels in Accordance with the Concentration of Guest Molecules. *J. Am. Chem. Soc.* **1998**, *120* (22), 5577−5578.

(4) Xiao, Y.; Lubin, A. A.; Heeger, A. J.; Plaxco, K. W. Label-Free Electronic Detection of Thrombin in Blood Serum by Using an Aptamer-Based Sensor. *Angew. Chem., Int. Ed.* **2005**, *44* (34), 5456−5459.

(5) Park, K. S.; Choi, A.; Kim, H. J.; Park, I.; Eom, M.-S.; Yeo, S.-G.; Son, R. G.; Park, T.-I.; Lee, G.; Soh, H. T.; Hong, Y.; Pack, S. P. Ultra-Sensitive Label-Free SERS Biosensor with High-Throughput Screened DNA Aptamer for Universal Detection of SARS-CoV-2 Variants from Clinical Samples. *Biosens. Bioelectron.* **2023**, *228*, No. 115202.

(6) Dauphin-Ducharme, P.; Yang, K.; Arroyo-Currás, N.; Ploense, K. L.; Zhang, Y.; Gerson, J.; Kurnik, M.; Kippin, T. E.; Stojanovic, M. N.; Plaxco, K. W. Electrochemical Aptamer-Based Sensors for Improved Therapeutic Drug Monitoring and High-Precision, Feedback-Controlled Drug Delivery. *ACS Sens.* **2019**, *4* (10), 2832−2837.

(7) Santos-Cancel, M.; Simpson, L. W.; Leach, J. B.; White, R. J. Direct, Real-Time Detection of Adenosine Triphosphate Release from Astrocytes in Three-Dimensional Culture Using an Integrated Electrochemical Aptamer-Based Sensor. *ACS Chem. Neurosci.* **2019**, *10* (4), 2070−2079.

(8) McKeague, M.; DeRosa, M. C. Challenges and Opportunities for Small Molecule Aptamer Development. *J. Nucleic Acids* **2012**, *2012*, 1−20.

(9) Varanko, A. K.; Su, J. C.; Chilkoti, A. Elastin-Like Polypeptides for Biomedical Applications. *Annu. Rev. Biomed. Eng.* **2020**, *22* (1), 343−369.

(10) Rembert, K. B.; Paterová, J.; Heyda, J.; Hilty, C.; Jungwirth, P.; Cremer, P. S. Molecular Mechanisms of Ion-Specific Effects on Proteins. *J. Am. Chem. Soc.* **2012**, *134* (24), 10039−10046.

(11) Qu, F.; Li, X.; Lv, X.; You, J.; Han, W. Highly Selective Metal−Organic Framework-Based Sensor for Protamine through Photo-induced Electron Transfer. *J. Mater. Sci.* **2019**, *54* (4), 3144−3155.

(12) Chen, Y.; Meng, X.-Z.; Gu, H.-W.; Yi, H.-C.; Sun, W.-Y. A Dual-Response Biosensor for Electrochemical and Glucometer Detection of DNA Methyltransferase Activity Based on Functionalized Metal-Organic Framework Amplification. *Biosens. Bioelectron.* **2019**, *134*, 117−122.

(13) Lanzalaco, S.; Mingot, J.; Torras, J.; Alemán, C.; Armelin, E. Recent Advances in Poly(*N* -isopropylacrylamide) Hydrogels and Derivatives as Promising Materials for Biomedical and Engineering Emerging Applications. *Adv. Eng. Mater.* **2023**, *25* (4), No. 2201303.

(14) Yim, H.; Kent, M. S.; Mendez, S.; Lopez, G. P.; Satija, S.; Seo, Y. Effects of Grafting Density and Molecular Weight on the Temperature-Dependent Conformational Change of Poly(*N* -Isopropylacrylamide) Grafted Chains in Water. *Macromolecules* **2006**, *39* (9), 3420−3426.

(15) Lubin, A. A.; Plaxco, K. W. Folding-Based Electrochemical Biosensors: The Case for Responsive Nucleic Acid Architectures. *Acc. Chem. Res.* **2010**, *43* (4), 496−505.

(16) Lee, K.; Povlich, L. K.; Kim, J. Recent Advances in Fluorescent and Colorimetric Conjugated Polymer-Based Biosensors. *Analyst* **2010**, *135* (9), 2179.

(17) Dang, J.; Guo, Z.; Zheng, X. Label-Free Sensitive Electrogenerated Chemiluminescence Aptasensing Based on Chitosan/$Ru(Bpy)_3^{2+}$/Silica Nanoparticles Modified Electrode. *Anal. Chem.* **2014**, *86* (18), 8943−8950.

(18) Scognamiglio, V.; Antonacci, A. Structural Changes as a Tool for Affinity Recognition: Conformational Switch Biosensing. *Crystals* **2022**, *12* (9), 1209.

(19) Sass, S.; Stöcklein, W. F. M.; Klevesath, A.; Hurpin, J.; Menger, M.; Hille, C. Binding Affinity Data of DNA Aptamers for Therapeutic Anthracyclines from Microscale Thermophoresis and Surface Plasmon Resonance Spectroscopy. *Analyst* **2019**, *144* (20), 6064−6073.

(20) Pietschnig, R. Polymers with Pendant Ferrocenes. *Chem. Soc. Rev.* **2016**, *45* (19), 5216−5231.

(21) Saleem, M.; Yu, H.; Wang, L.; Zain-ul-Abdin; Khalid, H.; Akram, M.; Abbasi, N. M.; Huang, J. Review on Synthesis of Ferrocene-Based Redox Polymers and Derivatives and Their Application in Glucose Sensing. *Anal. Chim. Acta* **2015**, *876*, 9−25.

(22) Lee, Y. Y.; Walker, D. B.; Gooding, J. J.; Messerle, B. A. Ruthenium(II) Complexes Containing Functionalised β-Diketonate Ligands: Developing a Ferrocene Mimic for Biosensing Applications. *Dalton Trans* **2014**, *43* (33), 12734−12742.

(23) Kang, H.; Liu, R.; Sun, H.; Zhen, J.; Li, Q.; Huang, Y. Osmium Bipyridine-Containing Redox Polymers Based on Cellulose and Their Reversible Redox Activity. *J. Phys. Chem. B* **2012**, *116* (1), 55−62.

(24) Vallée-Bélisle, A.; Plaxco, K. W. Structure-Switching Biosensors: Inspired by Nature. *Curr. Opin. Struct. Biol.* **2010**, *20* (4), 518−526.
(25) Plaxco, K. W.; Soh, H. T. Switch-Based Biosensors: A New Approach towards Real-Time, in Vivo Molecular Detection. *Trends Biotechnol.* **2011**, *29* (1), 1−5.
(26) Parolo, C.; Idili, A.; Ortega, G.; Csordas, A.; Hsu, A.; Arroyo-Currás, N.; Yang, Q.; Ferguson, B. S.; Wang, J.; Plaxco, K. W. Real-Time Monitoring of a Protein Biomarker. *ACS Sens.* **2020**, *5* (7), 1877−1881.
(27) Nawaz, N.; Abu Bakar, N. K.; Muhammad Ekramul Mahmud, H. N.; Jamaludin, N. S. Molecularly Imprinted Polymers-Based DNA Biosensors. *Anal. Biochem.* **2021**, *630*, No. 114328.
(28) Ertürk, G.; Mattiasson, B. Molecular Imprinting Techniques Used for the Preparation of Biosensors. *Sensors* **2017**, *17* (2), 288.
(29) Wu, Z.; Lin, D.; Li, Y. Pushing the Frontiers: Tools for Monitoring Neurotransmitters and Neuromodulators. *Nat. Rev. Neurosci.* **2022**, *23* (5), 257−274.
(30) Niyonambaza, S. D.; Kumar, P.; Xing, P.; Mathault, J.; De Koninck, P.; Boisselier, E.; Boukadoum, M.; Miled, A. A Review of Neurotransmitters Sensing Methods for Neuro-Engineering Research. *Appl. Sci.* **2019**, *9*, 4719.
(31) Moon, J.-M.; Thapliyal, N.; Hussain, K. K.; Goyal, R. N.; Shim, Y.-B. Conducting Polymer-Based Electrochemical Biosensors for Neurotransmitters: A Review. *Biosens. Bioelectron.* **2018**, *102*, 540−552.
(32) Wang, Y.; Mishra, D.; Bergman, J.; Keighron, J. D.; Skibicka, K. P.; Cans, A.-S. Ultrafast Glutamate Biosensor Recordings in Brain Slices Reveal Complex Single Exocytosis Transients. *ACS Chem. Neurosci.* **2019**, *10* (3), 1744−1752.
(33) Wang, Y.; Fathali, H.; Mishra, D.; Olsson, T.; Keighron, J. D.; Skibicka, K. P.; Cans, A.-S. Counting the Number of Glutamate Molecules in Single Synaptic Vesicles. *J. Am. Chem. Soc.* **2019**, *141* (44), 17507−17511.
(34) Ganesana, M.; Trikantzopoulos, E.; Maniar, Y.; Lee, S. T.; Venton, B. J. Development of a Novel Micro Biosensor for in Vivo Monitoring of Glutamate Release in the Brain. *Biosens. Bioelectron.* **2019**, *130*, 103−109.
(35) Nontipichet, N.; Khumngern, S.; Choosang, J.; Thavarungkul, P.; Kanatharana, P.; Numnuam, A. An Enzymatic Histamine Biosensor Based on a Screen-Printed Carbon Electrode Modified with a Chitosan−Gold Nanoparticles Composite Cryogel on Prussian Blue-Coated Multi-Walled Carbon Nanotubes. *Food Chem.* **2021**, *364*, No. 130396.
(36) Torre, R.; Costa-Rama, E.; Nouws, H. P. A.; Delerue-Matos, C. A Do-It-Yourself Electrochemical Cell Based on Pencil Leads and Transparency Sheets: Application to the Enzymatic Determination of Histamine. *Talanta* **2024**, *266*, No. 124980.
(37) Güçlü, K.; Özyürek, M.; Güngör, N.; Baki, S.; Apak, R. Selective Optical Sensing of Biothiols with Ellman's Reagent: 5,5′-Dithio-Bis(2-Nitrobenzoic Acid)-Modified Gold Nanoparticles. *Anal. Chim. Acta* **2013**, *794*, 90−98.
(38) Xiao, Y.; Lai, R. Y.; Plaxco, K. W. Preparation of Electrode-Immobilized, Redox-Modified Oligonucleotides for Electrochemical DNA and Aptamer-Based Sensing. *Nat. Protoc.* **2007**, *2* (11), 2875−2880.
(39) Ricci, F.; Lai, R. Y.; Heeger, A. J.; Plaxco, K. W.; Sumner, J. J. Effect of Molecular Crowding on the Response of an Electrochemical DNA Sensor. *Langmuir* **2007**, *23* (12), 6827−6834.
(40) Lo Nostro, P.; Ninham, B. W. Hofmeister Phenomena: An Update on Ion Specificity in Biology. *Chem. Rev.* **2012**, *112* (4), 2286−2322.
(41) Okur, H. I.; Hladílková, J.; Rembert, K. B.; Cho, Y.; Heyda, J.; Dzubiella, J.; Cremer, P. S.; Jungwirth, P. Beyond the Hofmeister Series: Ion-Specific Effects on Proteins and Their Biological Functions. *J. Phys. Chem. B* **2017**, *121* (9), 1997−2014.
(42) Kou, R.; Zhang, J.; Wang, T.; Liu, G. Interactions between Polyelectrolyte Brushes and Hofmeister Ions: Chaotropes versus Kosmotropes. *Langmuir* **2015**, *31* (38), 10461−10468.
(43) Zajforoushan Moghaddam, S.; Thormann, E. Hofmeister Effect on PNIPAM in Bulk and at an Interface: Surface Partitioning of Weakly Hydrated Anions. *Langmuir* **2017**, *33* (19), 4806−4815.
(44) Zhang, Y.; Furyk, S.; Bergbreiter, D. E.; Cremer, P. S. Specific Ion Effects on the Water Solubility of Macromolecules: PNIPAM and the Hofmeister Series. *J. Am. Chem. Soc.* **2005**, *127* (41), 14505−14510.
(45) Zhang, Y.; Furyk, S.; Sagle, L. B.; Cho, Y.; Bergbreiter, D. E.; Cremer, P. S. Effects of Hofmeister Anions on the LCST of PNIPAM as a Function of Molecular Weight. *J. Phys. Chem. C* **2007**, *111* (25), 8916−8924.

https://doi.org/10.1021/acsapm.4c00121
ACS Appl. Polym. Mater. 2024, 6, 5630−5641